PHYSICAL REVIEW B VOLUME 25, NUMBER 4 15 FEBRUARY 1982

Open-orbit magnetoresistance spectra of potassium

M. Huberman and A. W. Overhauser
Department of Physics, Purdue University, West Lafayette, Indiana 47907
(Received 25 September 1981)

A theory of the open-orbit magnetoresistance of potassium, discovered by Coulter and Datars, is developed. The open orbits caused by the multiple periodicities of a charge-density-wave (CDW) state are derived. Since a single crystal consists of domains, each having its CDW wave vector along one of 24 preferred axes, we employ effective-medium theory to calculate the magnetoresistance rotation pattern. The effects of domain texture and size are illustrated. The magnetic field at which open-orbit peaks appear depends on the domain size, which we find to be ~ 0.1 mm. The rotation pattern at 24 T is calculated in order to exhibit the detailed information that becomes available at extremely high fields. High-field experiments would aid in the determination of open-orbit directions and allow magnetic-breakdown studies of the energy gaps.

I. INTRODUCTION

The discovery of open-orbit magnetoresistance peaks in potassium by Coulter and Datars[1] shows that its Fermi surface is multiply connected. A charge-density-wave (CDW) structure[2,3] explains[4] the main features: the large number of open-orbit peaks, their field dependence, their width, and variations in the data from run to run.

The nonsaturating magnetoresistance of the alkali metals has been a long-standing puzzle.[5] Both the transverse and longitudinal magnetoresistance of potassium increase linearly with magnetic field in fields as high as 10 T.[6–9] Fear that this was an artifact caused by probes led to the development of inductive techniques,[9–11] which confirm the results of probe methods. Helicon-resonance experiments on intentionally deformed samples[10] make surface imperfections[12] an unlikely explanation. Voids can cause a linear magnetoresistance,[13] but the volume fraction required is known to be too high.[14] The linear magnetoresistance is observed in both polycrystalline and single-crystal samples. It depends upon sample preparation and history, varying by almost 2 orders of magnitude for differently prepared specimens and by about 50% for nominally the same specimens.[6,7,10]

The most revealing results have been obtained by the induced torque technique, a probeless method for measuring the magnetoresistance as a function of field orientation.[15] In this experiment (Fig. 1), a single-crystal sphere is suspended in a uniform magnetic field $\vec{H}$. Slow rotation of $\vec{H}$ (or the crystal) about the suspension axis induces circulating currents in the sample. The magnetic moment of the induced current interacts with $\vec{H}$, producing a torque about the suspension axis. The torque depends on the induced current, which in turn depends on the magnetoconductivity of the sample in the field $\vec{H}$.

Early experiments by Schaefer and Marcus[16] on potassium single crystals in fields up to 3 T showed a nonsaturating torque, having a twofold anisotropy. The high-field torque had four broad peaks in a 360° rotation pattern. The twofold symmetry contradicted the supposed cubic symmetry, implying a preferred direction in the crystal.

Holroyd and Datars[17] showed that, although the torque was always nonsaturating, its anisotropy depended on the sample preparation and treatment. The torque was isotropic when all surface oil on the sample was removed, but had a four-peak, twofold anisotropy when there was a nonuniform coat-

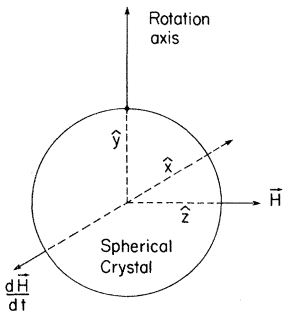

FIG. 1. Induced-torque experiment. Rotation of $\vec{H}$ induces currents, which interact with $\vec{H}$, producing a torque about the suspension axis.

ing of oil (oil-drop effect). The anisotropy cannot be blamed on sample shape or strain, since ellipsoidal and spherical samples had the same anisotropy, and intentionally strained samples showed no significant anisotropy. Voids or surface scratches cannot be the explanation, since deep cylindrical holes drilled into the sample had no significant effect.

In experiments at higher magnetic fields, Coulter and Datars[1] discovered narrow, nonsaturating torque peaks, appearing above about 5 T. The sharp structure was observed in approximately 100 runs on 12 specimens, when the torque at lower fields was either isotropic or anisotropic. The data for two crystals, about 4 mm in diameter, one grown in oil and the other in a mold, at a temperature 1.4 K are reproduced in Fig. 2. The magnetic field is in a (211) plane and a (321) plane, respectively, for Figs. 2(a) and 2(b).

Semiclassical transport theorems,[18] which are experimentally verified for many metals, predict that if a metal has only closed orbits, the high-field magnetoresistance saturates. For example, in copper crystals which are oriented in a magnetic field so that all orbits are closed, the predicted saturation of the magnetoresistance is observed.[19] A nonsaturating transverse magnetoresistance, proportional to H^2, can occur whenever $\vec{H}$ is perpendicular to an open-orbit direction. This effect disappears if $\vec{H}$ is rotated slightly into a nonperpendicular orientation. Sharp, nonsaturating magnetoresistance peaks, observed by rotating $\vec{H}$ (or the crystal), are the signature of open orbits.

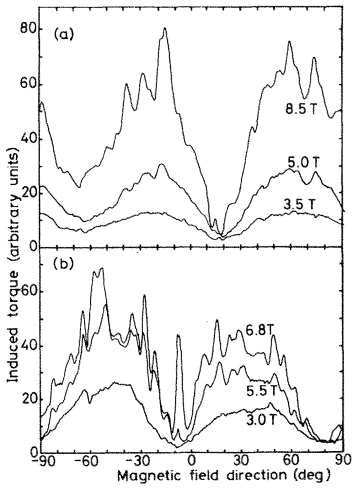

FIG. 2. Magnetoresistance of potassium versus $\vec{H}$ (Coulter and Datars, Ref. 1). (a) Single crystal grown in oil. $\vec{H}$ in the (211) plane; its direction in the plane of rotation is not known. (b) Single crystal grown in a *Kel-F* mold. $\vec{H}$ in the $(\bar{2}\,\bar{3}1)$ plane; its direction at $\theta=-90°$ is [128] and its sense of rotation is clockwise about the $[\bar{2}\,\bar{3}\,1]$ axis.

An exact solution for the induced torque in terms of the components of the magnetoresistivity tensor has been derived by Visscher and Falicov.[20] Assuming the high-field behavior predicted by semiclassical transport theorems,[18] the torque is approximately proportional to the magnetoresistance (ρ_{xx}) in the direction perpendicular to $\vec{H}$ and the rotation axis.[20] The induced-torque technique is thus an open-orbit detector, yielding sharp, nonsaturating torque peaks whenever $\vec{H}$ is perpendicular to an open-orbit direction.[15]

Potassium has a body-centered cubic lattice and is monovalent. The first Brillouin zone is only half-filled. The electrons at the Fermi surface are far from the zone boundary and their energy is only weakly perturbed by the lattice potential. The Fermi surface is expected to be nearly spherical and certainly simply connected. The occurrence of open orbits requires an additional periodic potential (besides the lattice potential), producing energy gaps at the Fermi surface.

In this paper we present a theory of the open-orbit magnetoresistance of potassium, shown in Fig. 2. We first review the theory of open-orbit magnetoresistance. The open-orbit directions in potassium, caused by a CDW, are then derived. The magnetoresistance of a single crystal, having a domain structure, is then calculated. We conclude with a discussion of directions for future research.

II. OPEN-ORBIT MAGNETORESISTANCE

We illustrate the theory of open-orbit magnetoresistance with a simple model: a Fermi surface consisting of two separate surfaces, a sphere and a cylinder.[21] This model has the virtue that its exact conductivity tensor is derivable.

In a magnetic field $\vec{H}=H\hat{z}$, the conductivity tensor $\vec{\vec{\sigma}}_s$ of a spherical Fermi surface is

$$\sigma_s=\sigma\begin{bmatrix}\dfrac{1}{1+(\omega_c\tau)^2} & \dfrac{-\omega_c\tau}{1+(\omega_c\tau)^2} & 0\\ \dfrac{\omega_c\tau}{1+(\omega_c\tau)^2} & \dfrac{1}{1+(\omega_c\tau)^2} & 0\\ 0 & 0 & 1\end{bmatrix}. \tag{1}$$

$\sigma=ne^2\tau/m$ is the zero-field conductivity,

$\omega_c \equiv eH/mc$ is the cyclotron frequency, and τ is the electron relaxation time.

The conductivity tensor $\vec{\sigma}_c$ of a cylindrical Fermi surface, having an axis $\hat{w}$, is most conveniently expressed in the uvw coordinate system, shown in Fig. 3, defined by $\hat{u}=(\hat{w}x\hat{y})/\sin\phi$ and $\hat{v}=\hat{w}x\hat{u}$. ϕ is the angle between $\hat{w}$ and $\hat{y}$ and θ is the angle between the projection of $\hat{w}$ in the xz plane and $\hat{z}$. In the uvw frame,

$$\sigma_c' = \sigma \begin{vmatrix} \frac{1}{1+\delta^2} & \frac{-\delta}{1+\delta^2} & 0 \\ \frac{\delta}{1+\delta^2} & \frac{1}{1+\delta^2} & 0 \\ 0 & 0 & 0 \end{vmatrix} , \tag{2}$$

where $\delta \equiv \omega_c \tau \sin\phi \cos\theta$. Transforming into the xyz frame,

$$\sigma_c = \tilde{S}\sigma_c' S , \tag{3}$$

where the orthogonal transformation matrix is

$$S \equiv \begin{vmatrix} -\cos\theta & 0 & \sin\theta \\ \cos\phi\sin\theta & -\sin\phi & \cos\phi\cos\theta \\ \sin\phi\sin\theta & \cos\phi & \sin\phi\cos\theta \end{vmatrix} . \tag{4}$$

Letting η be the electron fraction of the cylindrical Fermi surface, the total conductivity of a sphere and cylinder is

$$\vec{\sigma} = (1-\eta)\vec{\sigma}_s + \eta\vec{\sigma}_c . \tag{5}$$

The zero-field resistivity is approximately the same as for a spherical Fermi surface, but, in a magnetic field, the open-orbit electrons affect the resistivity dramatically.

Figure 4 shows the transverse magnetoresistance ρ_{xx} as a function of field strength and orientation. The open-orbit electron fraction is $\eta=0.001$ and the angle between the open-orbit direction $\hat{w}$ and the rotation axis $\hat{y}$ is $\phi=45°$. Sharp, nonsaturating

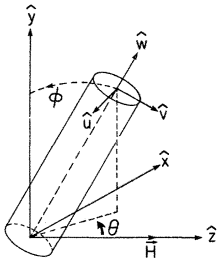

FIG. 3. Relative orientation of the uvw and xyz axes. $\hat{w}$ is the open-orbit direction and $\vec{H}$ is parallel to $\hat{z}$.

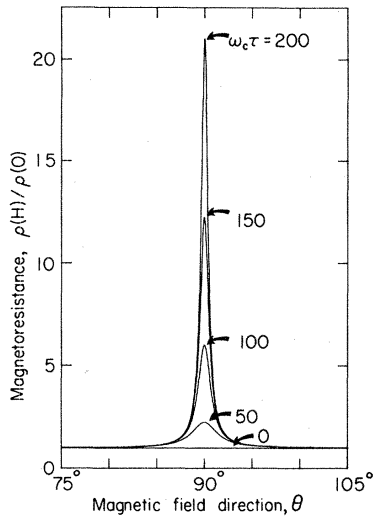

FIG. 4. Open-orbit magnetoresistance. Sharp peaks occur when $\vec{H}$ is perpendicular to the open-orbit direction $\hat{w}$. Open-orbit electron fraction $\eta=0.001$.

peaks, proportional to H^2, occur when $\vec{H}$ is perpendicular to $\hat{w}$. It can be shown that the peak height is

$$\Delta\rho_{xx} = [\eta/(1-\eta)]\rho(\omega_c\tau)^2\sin^2\phi , \tag{6}$$

where $\Delta\rho_{xx} \equiv \rho_{xx}(H) - \rho_{xx}(0)$ at $\theta=90°$ and $\rho \equiv 1/\sigma$. The peak fullwidth at half maximum, inversely proportional to H, is

$$\Delta\theta = 2/(\omega_c\tau\sin\phi) . \tag{7}$$

It can be shown that the Hall coefficient has the free-electron value, $R_H = -1/nec$. Open orbits have a negligible effect on the longitudinal magnetoresistance, which saturates when $\omega_c\tau > 1$.

III. OPEN-ORBIT DIRECTIONS

In a CDW state the conduction electron density has a sinusoidal modulation due to the effects of electron-electron interactions. The CDW wave vector $\vec{Q}$ in potassium has a magnitude[22] $Q \approx 1.33(2\pi/a)$, 8% larger than the Fermi surface diameter. Its theoretically predicted direction is near a [110] axis,[23] but because of elastic anisotropy, is tilted $\sim 4.1°$ away and lies in a plane oriented 65.4° away from the (001) plane.[24]

Due to the underlying cubic symmetry, there are 24 symmetry-related, preferred axes for $\vec{Q}$. Any single crystal will likely be divided into $\vec{Q}$ domains, each having its $\vec{Q}$ along one of these 24 axes. The domain distribution and size depend upon the

metallurgical history, being affected, for example, by sample shape and size, surface orientation and preparation, annealing time, and thermal stress. A directed stress due to a nonuniform oil drop or oxide spot can produce a preferred domain orientation. At temperatures above 15 K, where potassium begins its mechanical recovery,[25] domain growth can occur in order to relieve internal strains. The uncontrolled domain structure explains the variability of the open-orbit magnetoresistance for samples prepared by different methods and for the same sample after warming to liquid-nitrogen temperature.

The open orbits are created by three pairs of energy gaps, shown in relation to the Fermi surface in Fig. 5.[26] In a CDW state, the conduction electron density is

$$\rho(\vec{r})=\rho_0(1-p\cos\vec{Q}\cdot\vec{r}) . \tag{8}$$

ρ_0 is the average electron density; p and $\vec{Q}$ are the fractional modulation and wave vector of the CDW. The main gaps, which cause the 0.6 eV Mayer-El Naby optical-absorption anomaly,[22] arise from the exchange and correlation potential

$$V(\vec{r})=G\cos\vec{Q}\cdot\vec{r} \tag{9}$$

of the CDW. Since the CDW wave vector $\vec{Q}$ is only slightly larger than the Fermi-surface diameter, these gaps distort the Fermi surface nearby, forming small necks or points of critical contact.

The heterodyne gaps,[27] shown in Fig. 5, arise from a sinusoidal displacement of the positive ions, which occurs in order to maintain charge neutrality. The new ionic positions $\vec{R}_{\vec{L}}$ are related to the old positions $\vec{L}$ by

$$\vec{R}_{\vec{L}}=\vec{L}+\vec{A}\sin\vec{Q}\cdot\vec{L} . \tag{10}$$

$\vec{A}$ is the amplitude of the lattice distortion. Its magnitude is 0.03 Å and its direction is parallel to the vector (18.5,54.0,53.1) when $\vec{Q}=(2\pi/a)(0.966, 0.910,0.0865)$.[28] The ionic charge density is thus

$$\rho(\vec{r})=\sum_{\vec{L}}\bar{\rho}(\vec{r}-\vec{L}-\vec{A}\sin\vec{Q}\cdot\vec{L}) , \tag{11}$$

where $\bar{\rho}(\vec{r})$ is the charge density of a single ion at the origin and the sum is over all lattice sites $\vec{L}$.

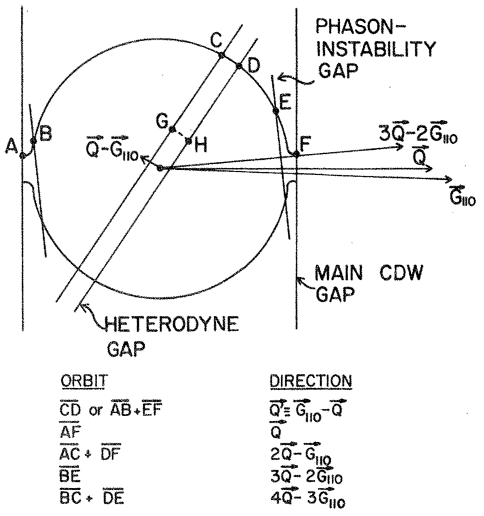

FIG. 5. Fermi surface, energy gaps, and open orbits of potassium (for $\vec{H}$ perpendicular to the plane shown).

The Fourier transform of $\rho(\vec{r})$ is

$$\rho_{\vec{q}}=\bar{\rho}(\vec{q})\sum_{\vec{L}}\exp[-i\vec{q}\cdot(\vec{L}+\vec{A}\sin\vec{Q}\cdot\vec{L})] , \tag{12}$$

where $\bar{\rho}(\vec{q})$ is the ionic form factor. Expanding to first order in the amplitude $\vec{A}$, we obtain

$$\rho_{\vec{q}}=\bar{\rho}(\vec{q})\sum_{\vec{L}}e^{-i\vec{q}\cdot\vec{L}}(1-i\vec{q}\cdot\vec{A}\sin\vec{Q}\cdot\vec{L}) \tag{13}$$

which is nonzero only if $\vec{q}=\vec{G}$ or $\vec{G}\pm\vec{Q}$, where $\vec{G}$ is any reciprocal lattice vector. Of the new periodicities $\vec{G}\pm\vec{Q}$, only $\vec{G}_{110}-\vec{Q}$ is smaller than the Fermi-surface diameter. Its energy gaps intersect the Fermi suface whereas those due to the others are not expected to do so.

The phason-instability gaps, also shown in Fig. 5, arise from a static phason instability,[29] having wave vector $2\vec{Q}$, which lowers the total energy. The ionic positions $\vec{R}_{\vec{L}}$ are now given by

$$\vec{R}_{\vec{L}}=\vec{L}+\vec{A}\sin(\vec{Q}\cdot\vec{L}+\beta\sin2\vec{Q}\cdot\vec{L}) , \tag{14}$$

where β is the amplitude of the static phason. Taking the Fourier transform of the ionic charge density and expanding to first order in $\vec{A}$ and β yields

$$\rho_{\vec{q}}=\bar{\rho}(\vec{q})\sum_{\vec{L}}e^{-i\vec{q}\cdot\vec{L}}[1-i\vec{q}\cdot\vec{A}(\sin\vec{Q}\cdot\vec{L}+\beta\cos\vec{Q}\cdot\vec{L}\sin2\vec{Q}\cdot\vec{L})] , \tag{15}$$

which is nonzero only if $\vec{q}=\vec{G}$, $\vec{G}\pm\vec{Q}$, or $\vec{G}\pm3\vec{Q}$, where $\vec{G}$ is any reciprocal lattice vector. Of the new periodicities $\vec{G}\pm3\vec{Q}$, four are smaller than the Fermi-surface diameter, producing energy gaps at the Fermi surface. Of these four, $3\vec{Q}-2\vec{G}_{110}$ is most longitudinal, i.e., has the largest component parallel to $\vec{A}$. Since $\rho_{\vec{q}}$ is proportional to $\vec{q}\cdot\vec{A}$, it is expected to have the largest energy gap.

Besides these, other energy gaps, which are higher order in the amplitudes $\vec{A}$ and β, occur. Except for the main gap, the sizes of these energy gaps are not known. In order to illustrate the theory, we include only the three sets of gaps shown in Fig. 5.

The main gap, which is 0.6 eV, is too large to be broken down by the magnetic field, but the others, which are smaller, may be. (The breakdown field for the main gap is about 1000 T.) The probability of an energy gap being broken down by a magnetic field $\vec{H}$ is[30]

$$P=\exp\left[-\frac{\pi mcE_g^2}{2\hbar^2 e\,|\,\vec{K}\cdot(\vec{v}\times\vec{H})\,|}\right] \equiv\exp\left[\frac{-H_0}{H}\right]. \tag{16}$$

$\vec{K}$ is the wave vector of the periodic potential producing the energy gap E_g and $\vec{v}$ is the velocity that an electron would have at the energy gap if it were free. Taking $\vec{H}$ parallel to $\hat{z}$ and $\vec{K}$ parallel to $\hat{x}$, Eq. (16) reduces to

$$P=\exp\left[-\frac{\pi E_g^2}{4\hbar\omega_c m\,|\,v_x v_y\,|}\right]. \tag{17}$$

Since the breakdown field H_0 depends on the electron velocity, an energy gap may simultaneously be broken down by some orbits on the Fermi surface and not by others.

Five open-orbit directions can be identified in Fig. 5. For example, if there is no magnetic breakdown, an electron traveling in k space on a cyclotron orbit from B to C will be Bragg reflected to D, will continue to E, where it will be Bragg reflected back to B. The open-orbit direction is $4\vec{Q}-3\vec{G}_{110}$. However, if the heterodyne gaps at C and D have suffered magnetic breakdown, the electron will travel continuously from B to E, where it will be reflected back to B. The open-orbit direction is then $3\vec{Q}-2\vec{G}_{110}$. A nonequatorial open orbit such as G to H (with reflection back to G) can occur even though the same heterodyne gaps have undergone magnetic breakdown on the equatorial orbit at C and D. The breakdown field of the orbit G to H, shown projected into the plane of Fig. 5, is greater than that of the orbit C to D, since $v_x v_y$ is less.

Since the magnitudes of the heterodyne and phason-instability gaps are not known, neither are the breakdown fields. Again, in order to illustrate the theory, we include all of the five possible open-orbit directions, indicated in Fig. 5.

IV. OPEN-ORBIT MAGNETORESISTANCE OF POTASSIUM

Obviously a theory for the angular dependence of the magnetoresistivity of a potassium crystal containing 24 types of $\vec{Q}$ domains, having therefore 120 open-orbit directions, must employ simplifying assumptions. We model the magnetoconductivity of a single domain as if it were caused by six Fermi-surface fractions, a sphere and five cylinders. The sphere contains $(1-5\eta)\approx 90\%$ of the conduction electrons. The cylinders, whose axes are parallel to the open-orbit directions in Fig. 5, each contain $\eta\approx 2\%$ of the conduction electrons.

Since the magnetic breakdown probability, given by Eq. (16), depends on the angle between $\vec{H}$ and the periodicity $\vec{K}$ producing the energy gaps, the open-orbit electron fraction η is different for each of the 120 open-orbit directions. Moreover it is field dependent, either increasing or decreasing as H increases. For example, as H increases, the electron fraction having the open-orbit direction $\vec{Q}$ will increase whereas that having the open-orbit direction $\vec{Q}'\equiv\vec{G}_{110}-\vec{Q}$ will decrease. In the model, 120 field-dependent values are thus replaced by one constant.

Since the energy gaps and breakdown fields are unknown, η cannot be estimated from the predicted Fermi surface (Fig. 5). We shall show, however, that the overall scale of the open-orbit magnetoresistance depends on η but the structure is insensitive to its value. Lacking absolute measurements of the induced torque, we assume the value $\eta\approx 2\%$.

Accordingly, the conductivity tensor for each type n of $\vec{Q}$ domain is given by

$$\overleftrightarrow{\sigma}_n=(1-5\eta)\overleftrightarrow{\sigma}_s+\eta\sum_{j=1}^{5}\overleftrightarrow{\sigma}_{cnj}. \tag{18}$$

$\overleftrightarrow{\sigma}_s$ is the magnetoconductivity tensor of a spherical Fermi surface, given by Eq. (1), and $\overleftrightarrow{\sigma}_{cnj}$ is the magnetoconductivity tensor of a cylindrical Fermi surface having an axis parallel to the jth open-orbit direction of $\vec{Q}$-domain n, given by Eqs. (2)–(4).

The conductivity tensor of a macroscopic single crystal, broken up into 24 $\vec{Q}$-domain varieties, is calculated by means of the effective medium approximation.[31,32] This is a mean-field type of approximation, which is expected to be valid when the domain size is greater than the electron mean free path but smaller than the sample dimensions. The effective conductivity tensor of the heterogeneous medium is[32]

$$\overleftrightarrow{\sigma}_{\text{eff}}=\overleftrightarrow{\sigma}_{\text{ext}} + \left[\sum_{n=1}^{24} f_n(\overleftrightarrow{\sigma}_n-\overleftrightarrow{\sigma}_{\text{ext}})\cdot\overleftrightarrow{\alpha}_n\right]\cdot\left[\sum_{n=1}^{24} f_n\overleftrightarrow{\alpha}_n\right]^{-1} . \tag{19}$$

f_n and $\overleftrightarrow{\sigma}_n$ are the volume fraction and conductivity of $\vec{Q}$-domain n. $\overleftrightarrow{\sigma}_{\text{ext}}$ is the conductivity of the "host" surrounding each domain. $\overleftrightarrow{\alpha}_n$ is a tensor depending on $\overleftrightarrow{\sigma}_n$ and $\overleftrightarrow{\sigma}_{\text{ext}}$, given by[33]

$$\overleftrightarrow{\alpha}_n=[\overleftrightarrow{1}-\overleftrightarrow{\Gamma}_{\text{ext}}\cdot(\overleftrightarrow{\sigma}_n-\overleftrightarrow{\sigma}_{\text{ext}})]^{-1} , \tag{20}$$

where the symmetric tensor $\overleftrightarrow{\Gamma}_{\text{ext}}$ depends only on the symmetric part $\overleftrightarrow{\sigma}^{(s)}_{\text{ext}}$ of $\overleftrightarrow{\sigma}_{\text{ext}}$, having the same principal axes. The eigenvalues Γ_i of $\overleftrightarrow{\Gamma}_{\text{ext}}$, which satisfy the equation

$$\sum_{i=1}^{3}\lambda_i\Gamma_i=-1 , \tag{21}$$

are functions of the eigenvalues λ_i of $\overleftrightarrow{\sigma}^{(s)}_{\text{ext}}$.[34] If $\lambda_1<\lambda_2<\lambda_3$, then

$$\Gamma_1=-\frac{1}{\lambda_1}\frac{1}{(\lambda_1\lambda_2\lambda_3)^{1/2}}\frac{1}{(1/\lambda_1-1/\lambda_3)^{1/2}(1/\lambda_1-1/\lambda_2)}(F-E) ,$$

$$\Gamma_3=-\frac{1}{\lambda_3}\frac{1}{(\lambda_1\lambda_2\lambda_3)^{1/2}}\frac{1}{(1/\lambda_1-1/\lambda_3)^{1/2}(1/\lambda_2-1/\lambda_3)}[(\lambda_3\lambda_1/\lambda_2)^{1/2}(1/\lambda_1-1/\lambda_3)^{1/2}-E] .$$

F and E are elliptic integrals of the first and second kinds, defined by

$$F(\delta,k)=\int_0^{\delta}(1-k^2\sin^2\phi)^{-1/2}d\phi ,$$

$$E(\delta,k)=\int_0^{\delta}(1-k^2\sin^2\phi)^{1/2}d\phi ,$$

having amplitude and modulus

$$\delta=\sin^{-1}(1-\lambda_1/\lambda_3)^{1/2} ,$$

$$k=\frac{(1/\lambda_1-1/\lambda_2)^{1/2}}{(1/\lambda_1-1/\lambda_3)^{1/2}} .$$

If $\lambda_1=\lambda_2<\lambda_3$, then $\Gamma_1=\Gamma_2$ and

$$\Gamma_3=-\frac{1}{\lambda_3-\lambda_1}\times\left[1-\frac{(\lambda_1/\lambda_3)^{1/2}\sin^{-1}(1-\lambda_1/\lambda_3)^{1/2}}{(1-\lambda_1/\lambda_3)^{1/2}}\right] .$$

If $\lambda_1<\lambda_2=\lambda_3$, then $\Gamma_2=\Gamma_3$ and

$$\Gamma_1=\frac{1}{\lambda_3-\lambda_1}\times\left[1-\frac{(\lambda_3/\lambda_1)^{1/2}\sinh^{-1}(\lambda_3/\lambda_1-1)^{1/2}}{(\lambda_3/\lambda_1-1)^{1/2}}\right] .$$

If $\lambda_1=\lambda_2=\lambda_3$, then $\Gamma_1=\Gamma_2=\Gamma_3=-\frac{1}{3}\lambda_3$.

The effective-medium approximation is obtained by requiring the conductivity $\overleftrightarrow{\sigma}_{\text{ext}}$ of the host, surrounding each domain, to be just $\overleftrightarrow{\sigma}_{\text{eff}}$. This self-consistent tensor,

$$\overleftrightarrow{\sigma}_{\text{eff}}=\overleftrightarrow{\sigma}_{\text{ext}} , \tag{22}$$

can be found quickly by iteration of Eq. (19). Starting from a free-electron conductivity tensor, the solution typically converged after five iterations to within 1%.

The 24 parameters f_n which specify the $\vec{Q}$-domain distribution are unknown. We take the $\vec{Q}$-domain distribution to be either random ($f_n=\frac{1}{24}$) or textured:

$$f_n=\tfrac{1}{24}\{1+\alpha[\tfrac{3}{2}(\hat{Q}\cdot\hat{T})^2-\tfrac{1}{2}]\} , \tag{23}$$

where $\hat{T}$ is the unit vector of the texture axis and α is a texture parameter lying between -1 and $+2$. $\alpha=0$ corresponds to no texture, $\alpha>0$ to a prolate texture, and $\alpha<0$ to an oblate texture.

The twofold anisotropy of the induced torque observed at lower magnetic fields, which contradicts the supposed cubic symmetry, shows that the $\vec{Q}$-domain distribution may have a preferred direction. Equation (23) is one example of such a distribution. In the model the 24 parameters f_n are thus replaced by three parameters, the texture axis $\hat{T}$ and texture parameter α. We shall show, however, that the main qualitative features of the open-orbit magnetoresistance do not depend on the assumed texture.

The electron scattering time τ at 1.4 K, which is primarily due to impurity scattering, is determined from the zero-field resistivity ρ. In zero magnetic field, the resistivity is approximately the same as for a spherical Fermi surface,

$$\rho=\frac{m}{ne^2\tau} , \tag{24}$$

since the cylindrical surfaces contain only a small fraction, $5\eta=10\%$, of the electrons. The zero-field resistivity of the induced-torque samples was

not measured, but the residual resistivity of pure potassium is typically about 4000 times smaller than the room-temperature resistivity $\rho=7\ \mu\Omega$ cm, implying $\tau\approx 1.5\times 10^{-10}$ sec at 1.4 K. Assuming this value, $\omega_c\tau=50$ at $H=2$ T.

The relaxation time τ applies to the spherical surface, having conductivity tensor $\overleftrightarrow{\sigma}_s$. In high magnetic fields, the open-orbit conductivity is much greater than the closed-orbit conductivity. Since an open-orbit is destroyed when it crosses a domain boundary, the relaxation time τ_{open} to be used in $\overleftrightarrow{\sigma}_{cnj}$ is shorter than τ. An electron in an open orbit travels in a straight line at the Fermi velocity v_F and the average distance it travels before leaving a spherical domain of diameter D is $3D/8$. τ_{open} is thus given approximately by

$$\frac{1}{\tau_{\text{open}}}=\frac{1}{\tau}+\frac{8v_F}{3D} \tag{25}$$

which may be rewritten as

$$\frac{\tau}{\tau_{\text{open}}}=1+\frac{8\lambda}{3D}\ , \tag{26}$$

where $\lambda=v_F\tau\approx 0.13$ mm is the electron mean free path. In principle, Eq. (25) applies only when $\vec{H}$ is nearly perpendicular to the open-orbit direction, but this modification has a small effect.

The magnetoresistivity ρ_{xx} for $\vec{H}$ in a plane perpendicular to a [211] or [321] axis was calculated according to the above theory and is shown in Fig. 6. Induced-torque curves were also calculated using the Visscher-Falicov formula[20] and are shown in Fig. 7. Except for the vertical scale, they are indistinguishable from the magnetoresistance curves. The crystal orientations in Fig. 6 correspond to the experimental data in Fig. 2. The crystallographic direction in the plane of rotation, which was not known for the data in Fig. 2(a), was adjusted in Fig. 6(a).

The magnetic field strength at which open-orbit peaks emerge depends somewhat on domain size. $D=0.05$ mm and $D=0.12$ mm were used, respectively, in Figs. 6(a) and 6(b); the corresponding open-orbit relaxation times are $\tau_{\text{open}}=\tau/8$ and $\tau_{\text{open}}=\tau/4$. A texture parameter $\alpha=-1$, with an axis at $\theta=0$, was used in Fig. 6(a); random orientation, $\alpha=0$, was used in Fig. 6(b).

A CDW domain structure is indeed consistent with the main features of the experimental results: the large number of open-orbit peaks, their field dependence, their width, and variations in the data from run to run. Since there is more than one open-orbit direction per domain, the peak locations

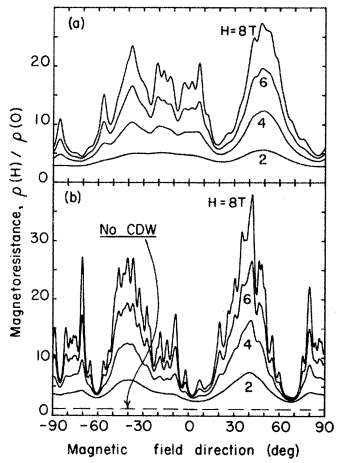

FIG. 6. Theoretical magnetoresistance versus $\vec{H}$. (a) $\vec{H}$ in the (211) plane; its direction at $\theta=-90°$ is $[\bar{1}20]$ and its sense of rotation is clockwise about the [211] axis. $D=0.05$ mm; texture: $\alpha=-1$, $\theta=0$. (b) $\vec{H}$ in the $(\bar{2}\bar{3}1)$ plane; its direction at $\theta=-90°$ is [128] and its sense of rotation is clockwise about the $[\bar{2}\bar{3}1]$ axis. $D=0.12$ mm; no texture ($\alpha=0$).

are not expected to correspond to a single set of 24 symmetry-related directions.

Magnetoresistance spectra for different open-orbit electron fractions η are shown in Fig. 8. The structure in the magnetoresistance is the same; only the overall scale is affected. Absolute meas-

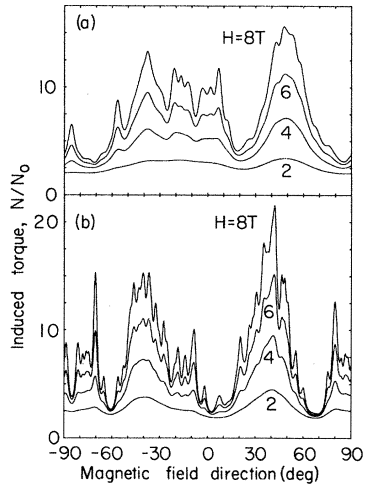

FIG. 7. Theoretical induced torque versus $\vec{H}$. The curves shown were *really* computed by the Visscher-Falicov formula, using the same parameters as in Fig. 6. For a spherical Fermi surface, the induced-torque saturates at $N_0=(8\pi/15)R^5\Omega(ne)^2\rho$, where ρ is the zero-field resistivity, n is the electron density, R is the sample radius, and Ω is the angular rotation frequency.

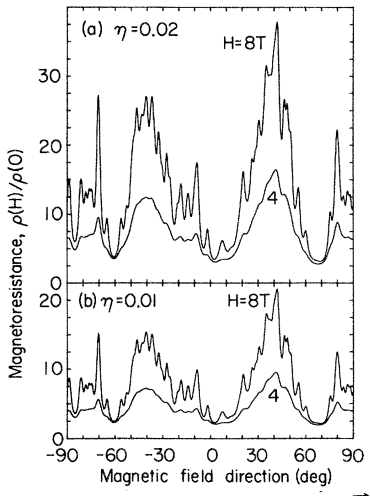

FIG. 8. Theoretical magnetoresistance for $\vec{H}$ in a (321) plane. (a) $\eta=0.02$. (b) $\eta=0.01$.

urements of the induced torque, together with the sample diameter, rotation frequency, and zero-field resistivity, will enable an estimate of η.

Magnetoresistance spectra for different textures are shown in Fig. 9. Although the qualitative features are the same, the quantitative details are very different. Some peaks present for one texture are absent for another. Until $\vec{Q}$-domain structure can be controlled, a detailed fit of theory and experiment is impossible, since it would require adjusting all 24 values of the domain probabilities f_n. The uncontrolled domain structure, both texture and size, explains the variability of induced-torque data.

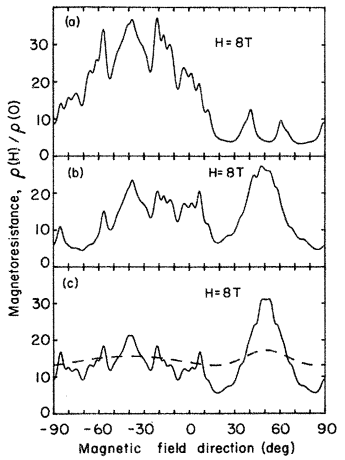

FIG. 9 Theoretical magnetoresistance for $\vec{H}$ in a (211) plane, $D=0.05$ mm. (a) $\alpha=2$, $\theta=60°$; (b) $\alpha=-1$, $\theta=0$; (c) $\alpha=0$. The dashed curve is for $D=0.005$ mm.

Magnetoresistance spectra for different domain sizes are shown in Fig. 10. $D=0.1$ mm in Fig. 10(b) is the approximate domain size of the experimental data in Fig. 2. If metallurgical preparation has caused too small a domain size, the open-orbit peaks can be suppressed. If the growth of larger domains is stimulated, about twice as many open-orbit peaks are clearly resolved. Induced-torque experiments thus provide a measure of the domain size.

V. DIRECTIONS FOR FUTURE RESEARCH

The immediate theoretical and experimental challenge is the determination of the open-orbit directions in potassium from its magnetoresistance spectra. Since the location of an open-orbit peak determines only the plane of the open-orbit direction, many experimental runs on accurately oriented crystals are required. If the temperature is allowed to rise above 15 K between runs, some peaks which are present in one run may be absent in the next due to domain distribution changes. Since only about 20 of the 120 predicted open-orbit peaks are present in Fig. 2, each observed peak contains many unresolved peaks, which further complicates the data analysis.

The additional information that becomes available at extremely high magnetic fields is illustrated in Figs. 11 and 12 by magnetoresistance spectra at

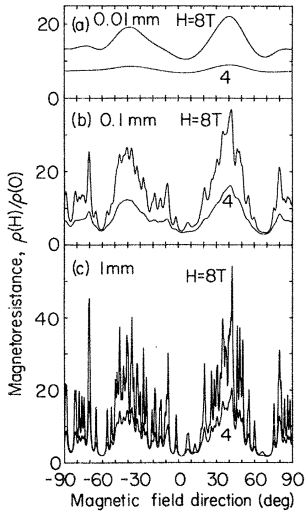

FIG. 10. Theoretical magnetoresistance for $\vec{H}$ in a (321) plane. (a) $D=0.01$ mm; (b) $D=0.1$ mm; (c) $D=1$ mm.

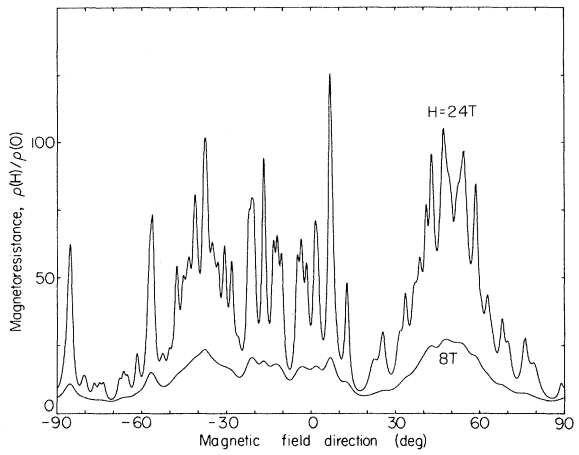

FIG. 11. Theoretical magnetoresistance at 24 T for $\vec{H}$ in a (211) plane.

24 T, which we have computed for $\vec{H}$ in a (211) or (321) plane. Approximately twice as many open-orbit peaks are sharply resolved at 24 T as at 8 T. We assumed as before that all five open-orbit directions in each $\vec{Q}$ domain are equally likely, even though magnetic breakdown may require this simple assumption to be modified. For example, if the heterodyne and phason-instability gaps can be neglected at such high fields, each $\vec{Q}$ domain would have only one open-orbit direction $\vec{Q}$, reducing the total number of open-orbit directions from 120 to 24. High-field experiments will thus also allow magnetic-breakdown studies of the energy gaps.

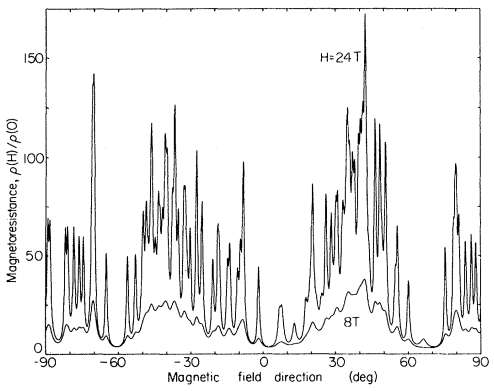

FIG. 12. Theoretical magnetoresistance at 24 T for $\vec{H}$ in a (321) plane.

VI. CONCLUSION

Potassium, the simplest metal of all, is for solid-state theory the analog of the hydrogen atom. Its properties must have explanations. Only two views are under serious consideration: (1) potassium has a CDW; (2) potassium has a spherical Fermi surface. The open-orbit magnetoresistance observed by Coulter and Datars,[1] shown in Fig. 2, supports the first view, which explains the main features, and rules out the second view, for which the only allowed magnetoresistance spectrum is the horizontal, dashed line shown in Fig. 6(b).

A question that is often asked is whether dislocations can cause the narrow torque peaks in Fig. 2. An oriented array of dislocations scatters electrons perpendicular to the dislocation axis. The total relaxation time due to impurity and dislocation scattering is then anisotropic. We have calculated the induced torque for oriented dislocations, assuming a zero-field resistivity

$$\overleftrightarrow{\rho}=\rho\begin{bmatrix}1&0&0\\0&1&0\\0&0&0.1\end{bmatrix} \tag{27}$$

which is 10 times less parallel to the dislocation axis than perpendicular to it. Taking the dislocation axis in the rotation plane, we show in Fig. 13 the dependence of the induced torque on the angle θ between $\vec{H}$ and the dislocation axis. The torque saturates at relatively low fields and is completely

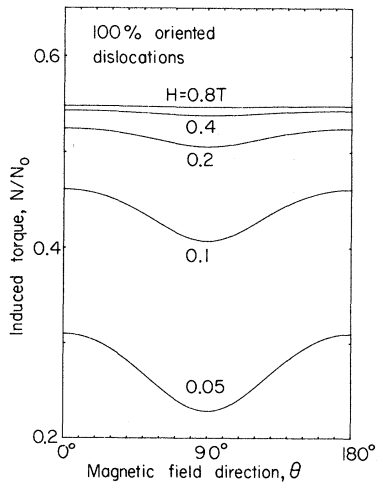

FIG. 13. Induced torque of oriented dislocations. Resistivity anisotropy=0.1. The torque saturates at $N/N_0=0.55$, where $N_0=(8\pi/15)R^5\Omega(ne)^2\rho$.

isotropic.[35]

An outstanding enigma is why the effects of a CDW are not observed in de Haas–van Alphen (dHvA) experiments. The dHvA frequency is proportional to the extremal Fermi-surface cross-sectional area. Although the pressure dependence of the dHvA frequency in potassium is anomalous,[36,37] its angular dependence is nearly isotropic.[38–40] The relatively large distortions of the Fermi surface near the energy-gap planes caused by a CDW are not observed.

Since the dHvA effect is sensitive only to closed orbits, it cannot detect the open orbits observed by the induced-torque technique. We expect that in a single domain sample the Fermi-surface anisotropy would be observed and can only conclude that the apparent isotropy is a consequence of the domain structure. We speculate that, if the $\vec{Q}$-domain size is small, the observed dHvA frequency is an average over many domains. A theory of the dHvA effect in a polydomain sample, taking into account electron-electron interactions, remains to be developed.

Deliberate attempts to prepare dHvA effect samples having large domain sizes are encouraged. The factors affecting the domain distribution in order of importance are surface orientation, directed stress, and a magnetic field. Surface faceting may control the domain size, since different surface orientations favor different $\vec{Q}$ directions. Etching, which produces larger facets, may thus stimulate the growth of larger domains. The small samples (about 1 mm in diameter) typically used in dHvA experiments may be "all surface"; their domain size may be limited by the surface facet size. The use of larger samples, having an interior region, may thus permit larger domains to grow. Simultaneous induced-torque measurements, interpreted using the theory developed here, would provide an estimate of the domain size.

We are grateful to the NSF-MRL program for support under Grant No. DMR77-23798.

---

[1]P. G. Coulter and W. R. Datars, Phys. Rev. Lett. 45, 1021 (1980); and private communication.
[2]A. W. Overhauser, Phys. Rev. 167, 691 (1968).
[3]For an experimental and theoretical review, see A. W. Overhauser, Adv. Phys. 27, 343 (1978).
[4]A brief exposition of this theory appeared in M. Huberman and A. W. Overhauser, Phys. Rev. Lett. 47, 682 (1981).
[5]E. Justi, Ann. Phys. (Leipzig) 3, 183 (1948); D. K. C. MacDonald, in *Handbuch der Physik,* edited by S. Flügge (Springer, Berlin, 1956), Vol. 14, p. 137.
[6]H. Taub, R. L. Schmidt, B. W. Maxfield, and R. Bowers, Phys. Rev. B 4, 1134 (1971).
[7]B. K. Jones, Phys. Rev. 179, 637 (1969).
[8]R. Fletcher, Phys. Rev. Lett. 45, 287 (1980).
[9]J. S. Lass, J. Phys. C 3, 1926 (1970).
[10]P. A. Penz and R. Bowers, Phys. Rev. 172, 991 (1968).
[11]A. M. Simpson, J. Phys. F 3, 1471 (1973). The interpretation of this experiment may require revision since an isotropic transverse resistivity was assumed.
[12]G. J. C. L. Bruls, J. Bass, A. P. van Gelder, H. van Kempen, and P. Wyder, Phys. Rev. Lett. 46, 553 (1981).
[13]D. Stroud and F. P. Pan, Phys. Rev. B 13, 1434 (1976).
[14]D. R. Schouten and C. A. Swenson, Phys. Rev. B 10, 2175 (1974); G. Stetter, W. Adlhart, G. Fritsch, E. Steichele, and E. Lüscher, J. Phys. F 8, 2075 (1978).
[15]J. S. Moss and W. R. Datars, Phys. Lett. 24A, 630 (1967). For an application to copper, see W. R. Datars, Can. J. Phys. 48, 1806 (1970).
[16]J. A. Schaefer and J. A. Marcus, Phys. Rev. Lett. 27, 935 (1971).
[17]F. W. Holroyd and W. R. Datars, Can. J. Phys. 53, 2517 (1975).
[18]I. M. Lifshitz, M. Ia. Azbel, and M. I. Kaganov, Zh. Eksp. Teor. Fiz. 31, 63 (1956) [Sov. Phys.—JETP 4, 41 (1957)]. For a theoretical and experimental review, see E. Fawcett, Adv. Phys. 13, 139 (1964).
[19]P. M. Martin, J. B. Sampsell, and J. C. Garland, Phys. Rev. B 15, 5598 (1977).
[20]P. B. Visscher and L. M. Falicov, Phys. Rev. B 2, 1518 (1970).
[21]A. W. Overhauser, Phys. Rev. B 9, 2441 (1974).
[22]A. W. Overhauser, Phys. Rev. Lett. 13, 190 (1964); A. W. Overhauser and N. R. Butler, Phys. Rev. B 14, 3371 (1976).
[23]A. W. Overhauser, Phys. Rev. B 3, 3173 (1971).
[24]G. F. Giuliani and A. W. Overhauser, Phys. Rev. B 20, 1328 (1979).
[25]W. S. C. Gurney and D. Gugan, Philos. Mag. 24, 857 (1971).
[26]In Fig. 5 the angle between $\vec{Q}$ and $\vec{G}_{110}$ is 2°. For the predicted tilt angle of 4.1°, the heterodyne and phason-instability energy-gap planes intersect on part of the Fermi surface. This complicates the figure, but does not change the open-orbit directions.
[27]J. R. Reitz and A. W. Overhauser, Phys. Rev. 171, 749 (1968).

[28]G. F. Giuliani and A. W. Overhauser, Phys. Rev. B 22, 3639 (1980); and private communication.
[29]G. F. Giulani and A. W. Overhauser, Bull. Am. Phys. Soc. 26, 471 (1981).
[30]E. I. Blount, Phys. Rev. 126, 1636 (1962); A. O. E. Animalu, *Intermediate Quantum Theory of Crystalline Solids* (Prentice-Hall, New Jersey, 1977).
[31]D. A. G. Bruggeman, Ann. Phys. (Leipzig) 24, 636 (1935); R. Landauer, J. Appl. Phys. 23, 779 (1952).
[32]D. Stroud and F. P. Pan, Phys. Rev. B 20, 455 (1979).
[33]D. Stroud and F. P. Pan, Phys. Rev. B 13, 1434 (1976).
[34]M. Huberman and A. W. Overhauser, Phys. Rev. B 23, 6294 (1981). In Eq. (20) of Ref. 34, the minus sign in Eq. (21) was inadvertently omitted.
[35]A. W. Overhauser, Phys. Rev. Lett. 27, 938 (1971).
[36]Z. Altounian, C. Verge, and W. R. Datars, J. Phys. F 8, 75 (1978); Z. Altounian and W. R. Datars, Can. J. Phys. 58, 370 (1980).
[37]I. M. Templeton, J. Low Temp. Phys. 43, 293 (1981).
[38]D. Shoenberg and P. J. Stiles, Proc. R. Soc. London Ser. A 281, 62 (1964).
[39]M. J. G. Lee and L. M. Falicov, Proc. R. Soc. London Ser. A 304, 319 (1968).
[40]M. J. O'Shea and M. Springford, Phys. Rev. Lett. 46, 1303 (1981).